Static and dynamic Jahn-Teller effects and antiferromagnetic order in PrO_2: A mean-field analysis

Jens Jensen
Niels Bohr Institute, Universitetsparken 5, 2100 Copenhagen, Denmark
(Received 7 June 2007; revised manuscript received 20 August 2007; published 24 October 2007)

The Pr ions in PrO_2 have a $4f^1$ configuration with a large orbital momentum and are placed in a strong crystalline field from the oxygen ions. Consequently, orbital effects dominate the magnetic properties of the system. At 120 K, there is a transition to a cooperative, oxygen-displaced Jahn-Teller phase, and the excitation spectra show clear evidences of the corresponding dynamical interaction. Below 13.4 K, the magnetic moments order in an antiferromagnetic structure, where one of the components is locked to the crystallographic Jahn-Teller distortion. A mean-field model is developed with the purpose of giving a unified description of these diverse properties of the compound. The paramagnetic phase is well described by the model, but a number of shortcomings in the account of the antiferromagnetic ordering suggest the presence of additional higher-order magnetic multipolar interactions.

DOI: 10.1103/PhysRevB.76.144428 PACS number(s): 75.10.Jm, 75.30.−m, 71.70.Ej

I. INTRODUCTION

The magnetic $5f$ electrons of the actinide ions in the dioxides UO_2 and NpO_2 show strong orbital effects due to the large crystalline field of the oxygen ions, antiferromagnetic and electrical quadrupolar ordering in UO_2,[1] and magnetic triakontadipoles (rank 5) ordering in NpO_2.[2] The $4f$ electrons in the lanthanide dioxide PrO_2 experience similar surroundings, and the orbital degree of freedom is also of vital importance for this compound. One unusual property of PrO_2 is that, due to the oxygen ions, the Pr ions are in the oxidation state Pr^{4+} with only a single electron left in the $4f$ shell.[3] In this $4f^1$ configuration, the orbital momentum, $L=3$, is large in comparison with the spin, $S=\frac{1}{2}$.

The overlap between the single $4f$ electron of a Pr ion and the electrons of the surrounding oxygen ions is weak. The oxygen ligand electrons are important for mediating the superexchange interactions between the $4f$ electrons on neighboring Pr ions, whereas the Jahn-Teller (JT) effects dominantly derive from the changes of the Coulomb field acting on the $4f$ electron due to displacements of external charges. This means that the decisive JT variables are the positions of the nuclei rather than the electrons of the oxygen ions. A static displacement of the oxygen ions affects the electronic $4f$ levels, as derived from the corresponding change of the crystal-field Hamiltonian, but does not mix the electronic and phonon coordinates. The mixing is only occurring when including the effects of the vibrational motions of the oxygen ions around their static equilibrium positions. This magnetoelastic coupling of the phonons and the magnetic excitations is the one named "the dynamic Jahn-Teller effect" in the case of a cooperative JT system (a general discussion of cooperative JT systems may be found in Ref. 4). This effect should not be confused with the dynamic JT effect of thermally activated tunneling between two different energy minima displayed by a local active JT ion.

Within the last few years, Boothroyd and co-workers have performed a comprehensive study of PrO_2.[3,5–8] Inelastic neutron scattering at 10 K on a polycrystalline sample showed peaks at about 131, 360, and 730 meV deriving from the crystal-field transitions and in addition, a broad peak centered at about 30 meV.[3] The latter one was interpreted as being due to a dynamic Jahn-Teller interaction. PrO_2 crystallizes in the fluorite structure with the cubic lattice parameter $a=5.392$ Å. Neutron-diffraction experiments on single crystals[6] revealed that the oxygen ions are displaced from their cubic symmetry positions below a second-order phase transition at $T_D=120$ K. The displacement becomes extremely large at low temperatures, where it is about 2.7% of the neighboring distance between the oxygen ions. PrO_2 is antiferromagnetically ordered below $T_N=13.4$ K with a type I component of about $0.65\mu_B$ per Pr ion at 2 K. This was first reported by Kern *et al.*;[9] however, the recent experiments[6] have uncovered that the antiferromagnetic moment has an additional component of about $0.35\mu_B$, which reflects the doubling of the unit cell of the JT distorted phase. The zero-temperature magnitude of the total antiferromagnetic moment of about $0.75\mu_B$ is a factor of 2 smaller than that deriving from a Γ_8 ground state. One possibility is that this quenching is caused by the mixing produced by the dynamic JT interaction of the phonon states and the magnetic Γ_8 state. The nature of the different phases has been analyzed in more detail by studying the changes of the domains caused by the application of a magnetic field,[7] and it is concluded that the field affects both the magnetic and the crystallographic domain patterns, and a spin-flip transition is observed when the field is applied along a [011] direction. It is most likely that both the JT displacements and the antiferromagnetic ordering are single-Q structures. In the paper published simultaneously with this one, Webster *et al.*[8] have determined the accurate symmetry of the JT structural phase and the temperature dependence of the polycrystalline excitation spectrum.

Here, I report an attempt to construct a mean-field model for PrO_2, which is in accordance with the experimental observations. The total angular momentum is $J=5/2$ and $g=6/7$ for the ground-state multiplet of the Pr^{4+} ions. Since the crystal-field anisotropy and the magnetoelastic JT energies are comparable with the splitting between the $J=5/2$ and $J=7/2$ multiplets, $(\frac{5}{2}+1)\zeta=375$ meV, the possible ef-

fects of the excited multiplet are included in the analysis by working within the total LS instead of the approximate $J=5/2$ basis. The Hamiltonian for each of the Pr ions in the undistorted cubic lattice is

$$\mathcal{H} = B_4[O_4^0(L) + 5O_4^4(L)] + B_6[O_6^0(L) - 21O_6^4(L)] + \zeta \mathbf{L}\cdot\mathbf{S} + \mu_B \mathbf{H}\cdot(\mathbf{L}+2\mathbf{S}). \quad (1)$$

General expressions for the Stevens operators may be found, for instance, in Refs. 10 and 11. The Jahn-Teller Hamiltonian is established in Sec. II. The mean-field (MF)–random-phase approximation (RPA) model for describing the behavior of PrO_2 in its paramagnetic phase is derived in Sec. III. The antiferromagnetic ordering is analyzed in Sec. IV, and the conclusions are given in Sec. V.

II. JAHN-TELLER HAMILTONIAN

The neutron-diffraction measurements[6] have shown that the crystal structure of PrO_2 is distorted below $T_D=120$ K. This distortion is considered to be a static Jahn-Teller effect induced by the derived change of the crystal-field anisotropy acting on the Pr ions. The diffraction experiments show that the Pr ions stay fixed, whereas the O ions are displaced so that the unit cell is doubled along a $\langle 100\rangle$ direction. Assuming the structural ordering wave vector to be along [100], the diffraction results determine the displacement vector of the oxygen ion at the position $\mathbf{R}$ to be

$$\mathbf{u}(\mathbf{R}) = \boldsymbol{\delta}_y \cos(\mathbf{Q}_{xy}\cdot\mathbf{R}+\phi_y) + \boldsymbol{\delta}_z \cos(\mathbf{Q}_{xz}\cdot\mathbf{R}+\phi_z). \quad (2)$$

The x, y, and z axes are defined to be along [100], [010], and [001], respectively. The two transverse displacement vectors are

$$\boldsymbol{\delta}_y = (0,\delta_y,0), \quad \boldsymbol{\delta}_z = (0,0,\delta_z), \quad \delta_y^2+\delta_z^2 = 2\delta^2, \quad (3)$$

and the wave vectors (in units of $\frac{2\pi}{a}$) are

$$\mathbf{Q}_{xy} = \left(\tfrac{1}{2},0,1\right), \quad \mathbf{Q}_{xz} = \left(\tfrac{1}{2},1,0\right) \quad (4)$$

The value of δ determined from the diffraction data[6] at 20 K is $\delta=0.0726$ Å.

The displacements of the O ions produce a change of the crystal-field Hamiltonian of the Pr ions linearly in the local strain field. The local strain field acting on a certain Pr ion, due to the displacement field $\mathbf{u}(\mathbf{R})$ in Eq. (2), may be obtained by averaging the relative displacements $\Delta u_\alpha/\Delta R_\beta$ of its eight neighboring O ions. Considering the Pr ion at [0, 0, 0], then its eight O neighbors are placed at $\left(\pm\frac{a}{4},\pm\frac{a}{4},\pm\frac{a}{4}\right)$. Defining $\theta_y=\mathbf{Q}_{xy}\cdot\mathbf{R}+\phi_y$ and $\theta_z=\mathbf{Q}_{xz}\cdot\mathbf{R}+\phi_z$ to be the total phase angles of the O ion at $\mathbf{R}=\left(-\frac{a}{4},-\frac{a}{4},-\frac{a}{4}\right)$, then the only nonzero symmetric component is

$$\epsilon_{yz} = \frac{1}{2}\left[\overline{\frac{\Delta u_y}{\Delta R_z}} + \overline{\frac{\Delta u_z}{\Delta R_y}}\right] = -\frac{\delta_y}{a}(\cos\theta_y - \sin\theta_y) - \frac{\delta_z}{a}(\cos\theta_z - \sin\theta_z). \quad (5)$$

The change of the crystal field produced by the antisymmetric component ω_{yz} is considered later on but is found to be negligible. The local strain field ϵ_{yz} deriving from $\mathbf{u}(\mathbf{R})$ may depend on the Pr ion considered. The lowest total energy is obtained when the value of ϵ_{yz}^2, averaged over the crystal, attains it maximum value for a certain cost of elastic energy, i.e., with the constraint that $\delta_y^2+\delta_z^2=2\delta^2$ is a constant. The average value of the squared strain determined from Eq. (5) is

$$\overline{\epsilon_{yz}^2} = \frac{1}{a^2}[\delta_y^2+\delta_z^2-2\delta_y\delta_z\sin(\theta_y+\theta_z)], \quad (6)$$

which is at its maximum when $\delta_y=\delta_z=\delta$ and $\theta_y+\theta_z=-\pi/2$. With a few exceptions (occurring when applying a field), the most stable of these configurations is the one minimizing the site variation of ϵ_{yz}^2, which leaves only one possibility (plus the equivalent ones generated by any integer values of p),

$$\theta_y = p\frac{\pi}{2}, \quad \theta_z = -(p+1)\frac{\pi}{2}, \quad \delta_y=\delta_z=\delta. \quad (7)$$

This is the chiral-displacement model shown in Fig. 1(b). The oxygen ions along a certain chain in the x direction are displaced in a chiral way; however, the sense of rotation changes from one chain to the next. Assuming the Pr ion in the lower right corner of the front to be the one at origin, then Fig. 1(b) shows the structure in the case of $\theta_y=\pi/2$. In the chiral structure, the value of ϵ_{yz}^2 is the same for all Pr ions, but the sign of ϵ_{yz} depends on the site considered. The variation of the sign is described by the wave vector $\mathbf{Q}_x=\mathbf{Q}_{xy}$, which is equivalent to $(-)\mathbf{Q}_{xz}$ when considering the Pr ions. With the choice of phase used in Fig. 1(b), then ϵ_{yz} is positive at the sites $x=0$, $\frac{3a}{2}$, $2a$, $\frac{7a}{2}$, $4a$, etc., and negative at the sites in between, when the Pr ions are those lying in the $y=0$ plane. In the next layer, at $y=\frac{a}{2}$, the signs are the opposite. Figure 1(a) shows the alternative, simple "sheared struc-

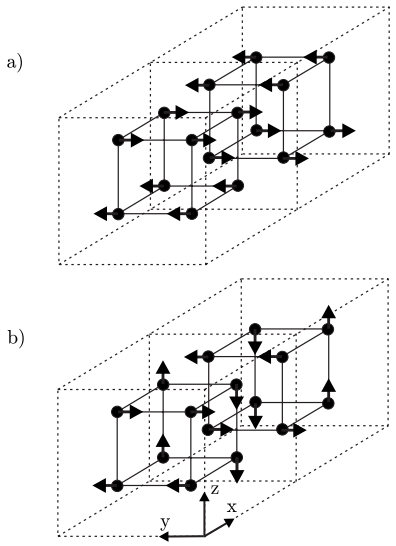

FIG. 1. Different displacement modes of the oxygen ions shown by arrows. The period of the displaced structure is two cubic unit cells along the x axis, and the two unit cells of the fcc lattice of the praseodymium ions are indicated by the dashed lines. (a) Sheared structure. (b) Chiral structure.

ture" ($\delta_y=\sqrt{2}\delta$, $\delta_z=0$, and $\theta_y=\pi/4$). In this structure, the magnetoelastic energy gain, proportional to ϵ_{yz}^2, is the same as in the chiral structure for half the Pr ions [those lying in the planes $x=(2p+1)\frac{a}{2}$] but zero for the other half, implying that this structure is unstable, both because of the large site variation of ϵ_{yz}^2 and because the energy gain is, in total, a factor of two smaller than for the chiral structure. Choosing instead $\theta_y=0$, then ϵ_{yz}^2 would be constant but the energy gain would still be a factor of 2 smaller than in the chiral case.

The Jahn-Teller term in the Hamiltonian of the ith Pr ion induced by the ϵ_{yz} strain of t_2 symmetry is

$$\mathcal{H}_{\mathrm{JT}} = -B_{\mathbf{u}}\epsilon_{yz}\hat{O}_2^{-1}(L) + \tfrac{1}{2}c_{\mathbf{u}}\epsilon_{yz}^2, \tag{8}$$

where $c_{\mathbf{u}}$ is a generalized elastic constant which accounts for the elastic energy (per Pr ion) associated with the chiral displacement of the oxygen ions. Here, the short hand notation is introduced:

$$\hat{O}_2^{-1}(L) = O_2^{-1}(L) + \alpha_4[O_4^{-1}(L) - 7O_4^{-3}(L)], \tag{9}$$

where the lowest-rank Stevens operator $O_2^{-1}(L)=\frac{1}{2}(L_yL_z+L_zL_y)$ [a minus (no) sign on the upper index m indicates that it is a sine (cosine) Stevens operator]. The analysis following below shows that the fourth-rank magnetoelastic coupling is, at least, as important as the second-rank one, and α_4 denotes the ratio between the two independent fourth- and the second-rank coupling parameters. The possible sixth-rank couplings may be neglected since the ground state is close to be the $J=5/2$ multiplet.

The JT Hamiltonian may be separated into a static phonon part and a dynamical one:

$$\mathcal{H}_{\mathrm{JT}} = \mathcal{H}_{\mathrm{JT}}^S + \mathcal{H}_{\mathrm{JT}}^D. \tag{10}$$

In order to do that, the thermal equilibrium condition for the static strain, $\partial F/\partial\epsilon_{yz}=\langle\partial\mathcal{H}_{\mathrm{JT}}/\partial\epsilon_{yz}\rangle=0$, is introduced in terms of the following equations:

$$E_{yz} = \frac{c_{\mathbf{u}}}{B_{\mathbf{u}}}\langle\epsilon_{yz}\rangle, \quad B_{2Q} = \frac{B_{\mathbf{u}}^2}{c_{\mathbf{u}}}, \tag{11}$$

with

$$E_{yz}^Q = \frac{1}{N}\sum_i \langle\hat{O}_2^{-1}(L_i)\rangle e^{-i\mathbf{Q}_x\cdot\mathbf{R}_i}, \tag{12a}$$

$$E_{yz} = E_{yz}(i) = E_{yz}^Q e^{i\mathbf{Q}_x\cdot\mathbf{R}_i} + (E_{yz}^Q)^* e^{-i\mathbf{Q}_x\cdot\mathbf{R}_i}. \tag{12b}$$

The two parts of the Hamiltonian for the ith ion are then obtained by replacing ϵ_{yz} in Eq. (8) by $\langle\epsilon_{yz}\rangle+(\epsilon_{yz}-\langle\epsilon_{yz}\rangle)$. The statistic part is independent of $(\epsilon_{yz}-\langle\epsilon_{yz}\rangle)$ and may be written

$$\mathcal{H}_{\mathrm{JT}}^S = -B_{2Q}E_{yz}\hat{O}_2^{-1}(L) + \tfrac{1}{2}B_{2Q}E_{yz}^2, \tag{13}$$

and the remaining part of $\mathcal{H}_{\mathrm{JT}}$ is the dynamical one,

$$\mathcal{H}_{\mathrm{JT}}^D = -B_{\mathbf{u}}(\hat{O}_2^{-1}(L) - E_{yz})(\epsilon_{yz} - \langle\epsilon_{yz}\rangle) + \tfrac{1}{2}c_{\mathbf{u}}(\epsilon_{yz} - \langle\epsilon_{yz}\rangle)^2. \tag{14}$$

The coupling constant B_{2Q} in the static Hamiltonian (13) is, per definition (11), positive. The sign of $\langle\hat{O}_2^{-1}(L_i)\rangle$ or of $E_{yz}(i)$ depends on the site considered, but the numerical value $|E_{yz}(i)|$ is going to be independent of i (at zero field) corresponding to $\theta_y=p\pi/2$ in Eq. (7). The dynamic Hamiltonian (14) may be rewritten by expanding the strain parameter in normal phonon coordinates β_1 and β_1^+. These phonon coordinates are defined with reference to the equilibrium positions of the oxygen ions before $\mathcal{H}_{\mathrm{JT}}^D$ is included. Since the thermal expectations values, per definition, are determined in terms of the total Hamiltonian, they include the effects of the dynamic part implying that $\epsilon_{yz}-\langle\epsilon_{yz}\rangle\propto\beta_1+\beta_1^+-\langle\beta_1+\beta_1^+\rangle$. Neglecting the dispersion of the normal phonon mode involved and adding the kinetic energies of the phonons, the dynamic JT Hamiltonian may be written as

$$\begin{aligned}\mathcal{H}_{\mathrm{JT}}^D = G\Big[&(\hat{O}_2^{-1}(L) - E_{yz})(\beta_1+\beta_1^+ - \langle\beta_1+\beta_1^+\rangle) + (\hat{O}_2^1(L) - E_{xz})\\ &\times(\beta_2+\beta_2^+ - \langle\beta_2+\beta_2^+\rangle) + \Big(\tfrac{1}{2}\hat{O}_2^{-2}(L) - E_{xy}\Big)(\beta_3+\beta_3^+\\ &- \langle\beta_3+\beta_3^+\rangle)\Big] + \frac{1}{2}\sum_{p=1,2,3}\hbar\omega_{\mathrm{JT}}\Big[(\beta_p\beta_p^+ + \beta_p^+\beta_p)\\ &- (\beta_p+\beta_p^+)\langle\beta_p+\beta_p^+\rangle + \tfrac{1}{2}\langle\beta_p+\beta_p^+\rangle^2\Big].\end{aligned} \tag{15}$$

The two additional terms involving $O_2^1(L)=\frac{1}{2}(L_xL_z+L_zL_x)$ and $O_2^{-2}=L_xL_y+L_yL_x$ are dictated by the cubic symmetry of the system. The effective operators introduced here are

$$\begin{aligned}\hat{O}_2^1(L) &= O_2^1(L) + \alpha_4[O_4^1(L) + 7O_4^3(L)],\\ \hat{O}_2^{-2}(L) &= O_2^{-2}(L) + \alpha_4[-4O_4^{-2}(L)].\end{aligned} \tag{16}$$

The dynamic JT Hamiltonian gives rise to a local mixing of the phonon modes, with t_2 symmetry, and the electronic $4f$ levels at the site i. This mixing affects the thermal expectation values, and since the Hamiltonian depends on such quantities, the calculations have to be performed in a self-consistent way. The appearance of $E_{yz}=\langle\hat{O}_2^{-1}(L)\rangle$ in the dynamic Hamiltonian gives rise to higher-order modifications, which are of some importance in the present strong-coupling system. The part of the phonon displacement induced by $\mathcal{H}_{\mathrm{JT}}^D$ is only nonzero if E_{yz} is nonzero, and the terms in Eq. (15) due to $\langle\beta_1+\beta_1^+\rangle$ have only minute effects on the thermal expectations values. Actually, the only effect found is that a neglect of $\langle\beta_1+\beta_1^+\rangle$ leads to a slightly improper behavior of the free energy close to T_N.

The same remarks apply to the terms deriving from the two other symmetry-related strain parameters, ϵ_{xz} or ϵ_{xy}. These terms may be introduced in the static Hamiltonian equivalent to the ϵ_{yz} term, but before doing that, I want to introduce two extensions of the JT Hamiltonian. At low temperatures, the structural displacements are large, implying that magnetoelastic couplings quadratic in the displacements may lead to significant effects. Based on symmetry arguments, assisted by an analysis of the point-charge model (see below), the leading terms in this order are found to be

$$\begin{aligned}\Delta_1\mathcal{H}_{\mathrm{JT}} = \eta B_{2Q}\{&[-O_2^0(L) + 3O_2^2(L)]E_{yz}^2\\ &+ [-O_2^0(L) - 3O_2^2(L)]E_{xz}^2 + 2O_2^0(L)E_{xy}^2\}\end{aligned} \tag{17}$$

and

$$\Delta_2\mathcal{H}_{\rm JT} = -\xi B_{2Q}\left\{\tfrac{1}{2}O_2^{-2}(L)E_{xz}E_{yz} + O_2^1(L)E_{xy}E_{yz} + O_2^{-1}(L)E_{xy}E_{xz}\right\}. \quad (18)$$

Including these higher-order terms, the total static JT Hamiltonian is

$$\mathcal{H}_{\rm JT}^S = -B_{2Q}\left[\hat{O}_2^{-1}(L)E_{yz} + \hat{O}_2^1(L)E_{xz} + \tfrac{1}{2}\hat{O}_2^{-2}(L)E_{xy}\right] + \tfrac{1}{2}B_{2Q}[E_{yz}^2 + E_{xz}^2 + E_{xy}^2] + \Delta_1\mathcal{H}_{\rm JT} + \Delta_2\mathcal{H}_{\rm JT}, \quad (19)$$

and the equilibrium condition, Eqs. (11) and (12), is modified into the following equations to be solved self-consistently:

$$E_{yz}^Q = \frac{1}{N}\sum_i \frac{\langle\hat{O}_2^{-1}(L_i)\rangle + \xi\left[\left\langle\tfrac{1}{2}O_2^{-2}(L_i)\right\rangle E_{xz}(i) + \langle O_2^1(L_i)\rangle E_{xy}(i)\right]}{1 + 2\eta\langle -O_2^0(L_i) + 3O_2^2(L_i)\rangle} \times e^{-i\mathbf{Q}_x\cdot\mathbf{R}_i}, \quad \mathbf{Q}_x = \left(\tfrac{1}{2},0,1\right), \quad (20a)$$

$$E_{xz}^Q = \frac{1}{N}\sum_i \frac{\langle\hat{O}_2^1(L_i)\rangle + \xi\left[\left\langle\tfrac{1}{2}O_2^{-2}(L_i)\right\rangle E_{yz}(i) + \langle O_2^{-1}(L_i)\rangle E_{xy}(i)\right]}{1 + 2\eta\langle -O_2^0(L_i) - 3O_2^2(L_i)\rangle} \times e^{-i\mathbf{Q}_y\cdot\mathbf{R}_i}, \quad \mathbf{Q}_y = \left(0,\tfrac{1}{2},1\right), \quad (20b)$$

$$E_{xy}^Q = \frac{1}{N}\sum_i \frac{\left\langle\tfrac{1}{2}\hat{O}_2^{-2}(L_i)\right\rangle + \xi[\langle O_2^1(L_i)\rangle E_{yz}(i) + \langle O_2^{-1}(L_i)\rangle E_{xz}(i)]}{1 + 2\eta\langle 2O_2^0(L_i)\rangle} \times e^{-i\mathbf{Q}_z\cdot\mathbf{R}_i}, \quad \mathbf{Q}_z = \left(1,0,\tfrac{1}{2}\right), \quad (20c)$$

where $E_{yz}(i)$ is determined as in Eq. (12b), and equivalently for the two other strain parameters. In these equations, I have assumed that the two quadratic coupling terms only depend on the local strain parameters. This assumption is fulfilled if the numerical values of the strain parameters are independent of i. In the exceptional cases where the numerical strain values are changing from site to site (between two different values), the point-charge model indicates that the local-interaction assumption is a better approximation than that obtained by the opposite choice of replacing the numerical strain values in Eqs. (17) and (18) by their averaged values.

The two quadratic coupling terms behave distinctly differently in the cases of a single-, double-, or triple-Q structural ordering. $\Delta_1\mathcal{H}_{\rm JT}$ has its strongest effect in the single-Q case and cancels out in the pure triple-Q case when $E_{xy}^2 = E_{xz}^2 = E_{yz}^2$. The quadratic couplings in $\Delta_2\mathcal{H}_{\rm JT}$ vanish in the single-Q case. At the first sight, it looks like these couplings would always favor the multiple-Q orderings when choosing suitable signs for the order parameters, but this is not the case. In order to understand this, we need to consider two effects. The first one is that the variation of, for instance, $\langle O_2^{-2}(L_i)\rangle$ induced by a nonzero $E_{xz}E_{yz}$ occurs at the wave vector $\left(\tfrac{1}{2},\tfrac{1}{2},0\right)$ and therefore does not have the same symmetry as E_{xy}. Hence, the total contribution of these coupling terms does not depend on the choice of signs for the order parameters, and it cancels out in the triple-Q case. The other effect to consider is that, independent of the quadratic couplings introduced by $\Delta_2\mathcal{H}_{\rm JT}$, then the quadrupole moment $\langle O_2^{-2}(L_i)\rangle$ is, in general, nonzero at the site i if $E_{xz}(i)$ and $E_{yz}(i)$ are both different from zero. This is a purely geometric effect appearing because the principal axes of O_2^{-1} and O_2^1 are not perpendicular to each other. The "inherent" quadrupole moment $\langle O_2^{-2}(L_i)\rangle$ is equal to a positive constant times $\langle O_2^1(L_i)\rangle \times\langle O_2^{-1}(L_i)\rangle$ and is thus proportional to $E_{xz}(i)E_{yz}(i)$. This means that the inherent quadrupole moment ordering has the same symmetry as that induced via $\Delta_2\mathcal{H}_{\rm JT}$ if ξ is nonzero. The triple-Q ordering is indifferent to a nonzero value of ξ, and the tendency for the formation of the inherent quadrupole moment is disguised by the third $\mathbf{Q}$ order parameter. In the double-Q case, the two effects may add constructively or the opposite, i.e., $\Delta_2\mathcal{H}_{\rm JT}$ may either favor or disfavor the double-Q ordering depending on the sign of ξ.

If δ_z in the chiral structure, as determined by Eq. (7), is replaced by $-\delta_z$, then the symmetric strain component ϵ_{yz} vanishes but is instead replaced by the antisymmetric one $\omega_{yz} = \pm 2\delta/a$. A nonzero value of this component corresponds to a rotation of the local coordinate axes by the angle $\theta = \tan^{-1}\omega_{yz} \simeq \omega_{yz}$ around the x axis. To first order in ω_{yz}, this rotation implements a new term in the Hamiltonian:[12]

$$\mathcal{H}_{\rm JT}(\omega_{yz}) = -20B_4\{O_4^{-1}(L) + O_4^{-3}(L)\}\omega_{yz} + \tfrac{1}{2}c_{\mathbf{u}}\omega_{yz}^2. \quad (21)$$

The additional sixth-rank term due to B_6 in the crystal-field Hamiltonian (1) is of no importance and is neglected. The equivalence of the local displacements in the two cases implies that the elastic energy associated with the antisymmetric displacement mode is the same as in the case of the symmetric strain mode, see Eq. (8). The different symmetry of the static displacements corresponding to either $\langle\epsilon_{yz}\rangle$ or $\langle\omega_{yz}\rangle$ implies that the system (in the paramagnetic phase) will choose the one or the other as the ordering parameter, leaving the alternative one to stay zero below the JT transition. Since the two phases only differ by a change of sign of, for instance, δ_z, they cannot be distinguished by the diffraction measurements; however, the analysis presented in the next section more or less rules out that the ordered phase is the $\langle\omega_{yz}\rangle$ phase.

III. MEAN-FIELD–RANDOM-PHASE-APPROXIMATION MODEL FOR PrO_2

The main parameters of the model, the spin-orbit coupling parameter ζ, the crystal-field parameters B_4 and B_6, and the dynamical JT interaction parameters G and $\hbar\omega_{\rm JT}$, have been derived from the fitting of the single-ion level scheme determined by inelastic neutron scattering on a polycrystalline sample.[3] B_{2Q} and α_4 are then determined by the crystallographic transition temperature $T_D = 120$ K and by the temperature variation of the Γ_7 doublet observed in the polycrystalline case.[8] If α_4 is neglected, the model predicts a strong first-order transition at T_D, in contradiction with the experiments, and an increase of the energy of the Γ_7 doublet by about 30 meV, when reducing the temperature from 120 to 10 K, which is a factor of 3 larger than observed by Webster *et al.*[8] Assuming a nonzero α_4, the transition is quickly modified to become of second order, and about the right temperature shift of the Γ_7 doublet is obtained when α_4 is less than $-1.5\alpha_4^0$ or greater than $3\alpha_4^0$, where $\alpha_4^0 = 0.005\,24$ is the value predicted by the point-charge model. The magnetic anisotropy predicted, in the case of a single-Q struc-

TABLE I. The main parameters of the mean-field model. Except for the pure number α_4, all the parameters are in units of meV.

ζ	B_4	B_6	G	$\hbar\omega_{\mathrm{JT}}$	B_{2Q}	α_4
103	−0.338	−0.0149	4.8	40	3.7	0.02

tural ordering, is in disagreement with experiments when $\alpha_4 < -1.5\alpha_4^0$ or when $\alpha_4 > 5\alpha_4^0$. Hence, these comparisons indicate that $3\alpha_4^0 < \alpha_4 < 5\alpha_4^0$.

In order to secure that the parameters derived in the analysis are not completely unrealistic, I have compared their values with that predicted by a straightforward point-charge model[10] in which the Pr and O ions have been replaced by point charges of $4e$ and $-2e$, respectively. This model predicts B_4 to be a factor of 2.6 and B_6 to be a factor of 4.4 smaller than derived from experiments. Assuming a systematic multiplicative correction factor of the point-charge predictions, which depends only on l, then $\alpha_4 \approx 4\alpha_4^0$ appears to be the most acceptable possibility, which suggests a scaling of the point-charge predictions by about $2.6/4=0.65$ when $l=2$. This estimate is in accordance with that derived from a direct comparison between experiments and predictions, and in the final model, I use $\alpha_4=0.02 \simeq 3.8\alpha_4^0$. Incidentally, according to the point-charge model, E_{yz} and ϵ_{yz} have opposite signs at a certain site, but this has no influence on any of the arguments. The point-charge model seems to be reasonably trustworthy, and assuming the fourth-rank scale factor to be of the order of 3, then it predicts that the additional magnetoelastic coupling introduced by Eq. (21) is of no importance. The alternative structural ordering, with $\langle\omega_{yz}\rangle$ replacing $\langle\epsilon_{yz}\rangle$, is not relevant as the coupling constant is a factor of 3 too small, and the additional contributions to the dynamic JT Hamiltonian only have minute effects. It may be added that $\delta=0.0726$ corresponds to $\langle\omega_{yz}\rangle=0.027$ or a rotation of the crystal-field Hamiltonian by 1.5°, which is a rather slight effect. The two order parameters are coupled in the antiferromagnetic phase, but the effects due to the ω_{yz} terms are negligible also in this phase. Hence, all the additional contributions due to the antisymmetric part of the strain mode are minute and are neglected in the final calculations.

The model parameters derived from the fitting procedure are given in Table I. The calculated excitation spectrum[11] of a single Pr ion placed in the mean field of its surroundings is shown in Fig. 2. This corresponds closely to an RPA calculation of the directionally averaged spectrum of a polycrystalline sample. Figure 3 shows the calculated variation of the squared order parameter $E_{yz}^2(T)$ and the corresponding variation of the energy of the Γ_7 doublet. Most of these results are in reasonable agreement with experiments. The lowest peak in the polycrystalline spectrum at 10 K is due to the splitting of the Γ_8 quartet into two doublets because of the structural quadrupolar ordering. The peak is calculated to lie at about 19 meV at 10 K, to be compared with the experimental value of about 28 meV.[3,8] The temperature variation of the splitting is calculated to be roughly proportional with the order parameter $E_{yz}(T)$, which is in agreement with the observations, see Fig. 6 of Ref. 8. The experiments at 10 K of Boothroyd *et al.*[3] also detected a small shoulder on the Γ_7 peak, at an energy of about 160 meV, which may correspond to the calculated minor peak at about 180 meV. The calculated intensity between 30 and 120 meV is due to the dynamical

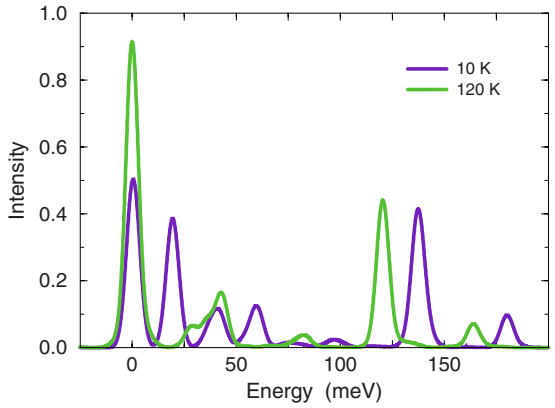

FIG. 2. (Color online) The excitation spectrum of polycrystalline PrO_2 calculated at 10 and at 120 K with a Gaussian resolution of $\sigma=3$ meV. The higher energy part of the spectrum (at 10 K) shows peaks at 360 and 730 meV in accordance with the observation of Boothroyd *et al.* (Ref. 3).

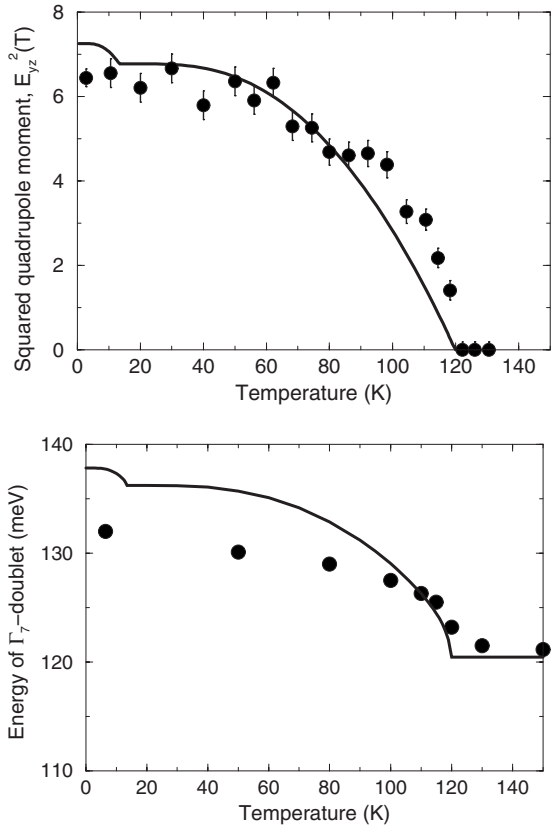

FIG. 3. The upper figure shows the square of the structural order parameter $E_{yz}^2(T)$ compared with the scaled intensity variation of the neutron scattering peak at (1/2,1,4) from Ref. 6. The lower figure shows the calculated temperature variation in the position of the Γ_7 scattering peak. The solid circles are the experimental results of Webster *et al.* (Ref. 8).

mixing between the Einstein phonon modes and the magnetic ones. The presence of this intermediate scattering intensity is in qualitative agreement with the observations; however, the experimental intensity is much more smeared out and does not show the distinct peaks. This discrepancy is probably related to the neglect of dispersive effects in the account of the dynamic JT interaction.

The leading order effects of the dynamic JT Hamiltonian (15) are accounted for by including the interactions between the states where no phonons are excited, $(n_1,n_2,n_3)=(0,0,0)$, to the states where only a single phonon is excited, i.e., where $(n_1,n_2,n_3)=(1,0,0)$, (0,1,0), or (0,0,1). Bevilacqua *et al.*[13] have found that the interactions to the multiple-excited phonon states, $n_\Sigma=n_1+n_2+n_3>1$, are important, particularly for the magnetic scattering intensities of the extra phononlike peaks induced by the Jahn-Teller coupling. Including successively the interactions for which $n_\Sigma \leqslant 1$, 2, 3, and 4, the calculations showed relatively large differences when including the states with $n_\Sigma=2$ compared to the case of $n_\Sigma \leqslant 1$, but only minor changes in the next step when adding the states for which $n_\Sigma=3$. Hence, this systematic behavior indicates that all effects of the excited phonon states are accurately implemented in the calculations by including all states for which $n_\Sigma \leqslant 4$. This implies a single-ion Hamiltonian matrix of dimension $14\times(1+3+6+10+15)=490$, a large but still manageable number. Although the effects of the excited phonon states are accurately included, the model calculations are still based on the rather crude approximation of nondispersive phonon modes.

The assumption that the static and dynamic JT effects have the same origin means that the values of the static and the dynamical JT parameters should be related. A rough estimate of the relationship may be derived by assuming an effective force constant K determining the Einstein frequency of the transverse oxygen mode by $\omega^2=K/M$, where M is the mass of an oxygen atom. K may then be derived from the elastic energy involved in the displacement field, $K\delta^2=\frac{1}{2}B_{2Q}E_{yz}^2$, which energy is determined from the model calculations to be about 13.5 meV (at zero temperature). This approach indicates that $\hbar\omega_{\mathrm{JT}}=\hbar\omega$ should be about 25 meV. Knowing the energy $\hbar\omega$ of the Einstein mode, the dynamical JT coupling constant in Eq. (15) is estimated to be $G=\sqrt{B_{2Q}\hbar\omega}=10$ meV. Considering that the dynamical coupling parameter is an effective one, which is going to be quite strongly modified (reduced) by dispersive effects, the agreement, within a factor of 2, between the parameter derived from this estimate and the one used in the model is convincing.

IV. ANTIFERROMAGNETIC PHASE

The system is found to order antiferromagnetically below 13.4 K. The main component is of type I, a transversely polarized ordering of the magnetic moments at the wave vectors $\langle 001\rangle$. The recent neutron-diffraction experiments have detected an additional weaker component at the wave vectors $\langle \frac{1}{2}01\rangle$.[6] The simplest possible model for explaining these observations is to assume a single-Q ordering of the oxygen displacements that creates an easy magnetic plane perpendicular to the structural ordering vector $\mathbf{Q}_\alpha$. The classical dipole interaction is unimportant, and considering that each cube of the four oxygen ions is shared between three pairs of nearest and one pair of next-nearest neighbors of Pr ions, the superexchange between these ions is expected to dominate the magnetic Hamiltonian, i.e., that

$$\mathcal{H}_{\mathrm{ex}}=-\frac{1}{2}\sum_{i,j\in p\mathrm{th\ nn}} J_p\mathbf{S}_i\cdot\mathbf{S}_j \tag{22}$$

with $p=1$ and 2. If only J_1 is important and is negative, the system would order antiferromagnetically with the moments lying in the easy plane perpendicular to $\mathbf{Q}_\alpha$. Considering the case $\mathbf{Q}_\alpha=\mathbf{Q}_x$, then E_{yz} is nonzero and is changing its sign from one site to the next. Thus, within the easy yz plane, there will be an easy direction that alternates between [0,1,1] and $[0,1,-1]$, as determined by the wave vector $(\frac{1}{2},0,1)$. In the case where J_1 is the dominating interaction, the Fourier transform of the exchange interaction $J(\mathbf{q})$ is equal to $-4J_1$ both at $\mathbf{q}=(1,0,0)$ and at $\mathbf{q}=(\frac{1}{2},0,1)$. This degeneracy allows the system to take full advantage of the anisotropy and the exchange energy simultaneously. One of the transverse component, e.g., the y component, will be ordered at the wave vector (1,0,0), whereas the variation of the other, the z component, is determined by the wave vector $(\frac{1}{2},0,1)\equiv\mathbf{Q}_x\pm(1,0,0)$, and the two components should be of equal magnitude. In general, when more exchange constants are important, the exchange fields acting on the two components are different from each other, and assuming $J((1,0,0))>J((\frac{1}{2},0,1))$, the length of the (1,0,0) or y component is going to be larger than the length of the $(\frac{1}{2},0,1)$ or z component, which is the antiferromagnetic ordering shown in Fig. 4(b). This magnetic structure is characterized by a single order parameter, the total length of the moment at a single site, and a direction of this moment determined by the ratio between the lengths of the two components. Since the two components are ordered at different wave vectors, the exchange field is, effectively, anisotropic, and the direction of the moments at a certain site is a compromise between the alternating easy $\langle 011\rangle$ directions of the single-ion anisotropy and the y direction favored by the exchange fields. The ordered magnetic structure shown in Fig. 4(a), as well as in Fig. 4(b), is concordant with the symmetry elements of the paramagnetic phase, and, within the framework of the Landau theory, the magnetic phase transition should be of second order. The magnetic structure removes the paramagnetic equivalence between the y and z directions, implying instead the presence of two magnetic domains in each of the single-Q structural domains.

The diffraction experiments on PrO_2 at 2 K show that the length of the (1,0,0) component is $\mu_1\simeq 0.65\mu_B$ and that the other is nearly a factor of 2 smaller, $\mu_2\simeq 0.35\mu_B$.[6] The simple model may be able to account for a difference between the two components only when including couplings J_p to other neighbors ($p\geqslant 2$). The model to be considered is

$$J_1=-2.25,\quad J_3=-1.0,\quad J_5=2.0, \tag{23}$$

all values in meV. The important point is not the actual values of these parameters, but rather that they lead to a large

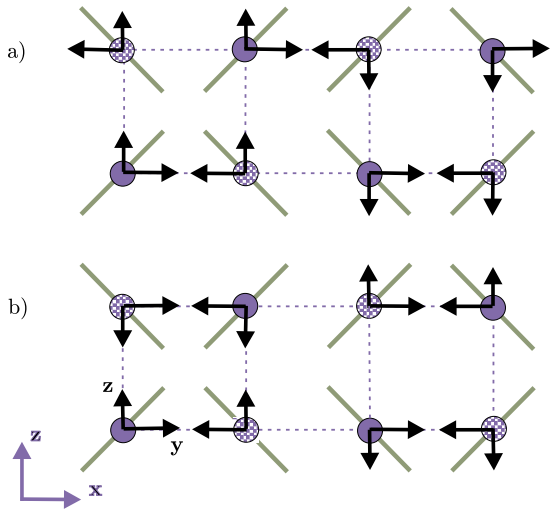

FIG. 4. (Color online) One period of the different antiferromagnetic orderings induced by the easy axes (designated by green lines in the local yz plane) established by the single-Q structural ordering along the x axis, $\mathbf{Q}_\alpha=\mathbf{Q}_x=(\frac{1}{2},0,1)$. The solid circles are the Pr ions of the $y=0$ face in the two cubic unit cells along the x axis (in the global xz plane), and the dashed ones are those lying in the $y=\frac{a}{2}$ plane. The ordered moments (black arrows) have a transverse type I component polarized along the local y axis. In case (a), the ordering wave vector is assumed to be perpendicular to the x axis, i.e., $\mathbf{q}_y=(0,0,1)$, and in case (b), $\mathbf{q}_y=(1,0,0)$ is parallel to x. The corresponding z component is then determined by the easy axes and is described by the wave vector $\mathbf{q}_z=(\frac{1}{2},0,0)$ in case (a) and $\mathbf{q}_z=(\frac{1}{2},0,1)$ in case (b).

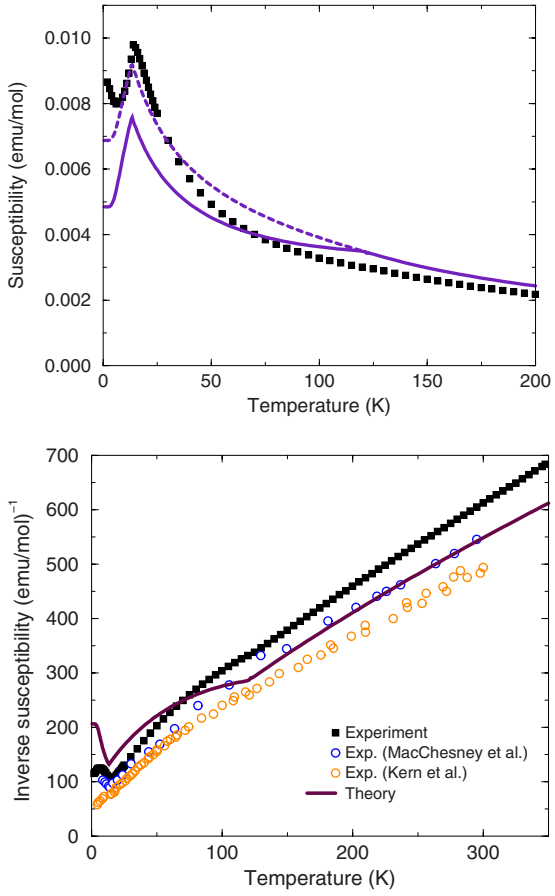

FIG. 5. (Color online) The calculated susceptibility using the model specified by Table I and Eq. (23). The experimental powder results denoted by the solid squares are from Ref. 6, which are compared with previous results of Kern (Ref. 14) and MacChesney *et al.* (Ref. 15). The solid lines show the average value of the magnetic susceptibility calculated when assuming an equal population of the three different crystallographic single-Q domains. In the upper figure, the dashed line shows the result if only the most favorable domains, with $\mathbf{Q}$ nearly perpendicular to the field, are present.

difference between $J((1,0,0))=33$ meV and $J((\frac{1}{2},0,1))=-15$ meV $>J((\frac{1}{2},0,0))=-17$ meV. The latter inequality is required in order to prevent stabilization of the alternative magnetic ordering shown in Fig. 4(a), where the type I ordering wave vector is perpendicular to $\mathbf{Q}_x$. In this case, the second transverse component would order at the wave vector $(\frac{1}{2},0,0)$, which is in disagreement with the observations. The model defined by Table I and the exchange constants in Eq. (23) predicts $\mu_1=0.868\mu_B$ and $\mu_2=0.564\mu_B$ at 2 K. The ratio $\mu_2/\mu_1=0.65$ is close to the experimental value of ~ 0.54, but the length of the moment of $1.035\mu_B$ is $\sim 40\%$ larger than the experimental one. The model calculations predict the ratio μ_2/μ_1 to stay nearly constant in the whole interval between the second-order phase transition at T_N and zero temperature. This is consistent with the observed behavior of the scattering intensities at (1,0,0) and $(\frac{1}{2},0,1)$, see Fig. 4 of Ref. 6.

The magnetic susceptibility predicted by this model is compared with experiments in Fig. 5. The high-temperature slope of the inverse susceptibility is calculated to be smaller than observed. This discrepancy is hard to explain, as the theoretical slope is more or less fixed by the position of the Γ_7 doublet [and the total length of the Pr moment, $(L+2S)\mu_B$], which is well determined by the model, see Fig. 3. As shown in Fig. 5, the calculated results compare with the experimental results of Kern[14] and MacChesney *et al.*,[15] which, however, seem to be influenced[16] by various contents of Pr_6O_{11} (possibly 20% in the case of the results of Kern).

The domain effects observed by Gardiner *et al.*, when the field is applied along [001],[7] are in accordance with the predictions of the present model. The magnetic energies are small compared to those involved in the structural deformations, as reflected in the values of the two transition temperatures, implying that the magnetic domain distribution is more sensitive than the crystallographic one. Hence, at low values of an applied field, only the populations of the different magnetic domains are going to change. In the two structural domains, where $\mathbf{Q}_\alpha$ is perpendicular to the field, the magnetic domains where the type I moment is parallel to the field has the largest susceptibility (i.e., the lowest energy at finite field), implying that half the magnetic domains in these two structural phases are going to be removed at relative low values of the field (experimentally of the order of 1 T), whereas nothing happens at low fields in the third structural domain in which $\mathbf{Q}_\alpha$ is along the field. This leads to an increase of the susceptibility by nearly 20%. At higher values

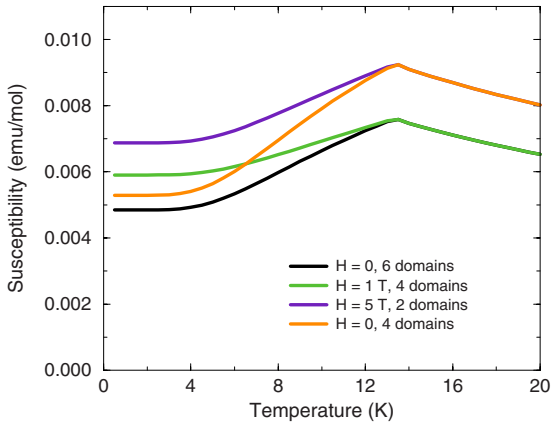

FIG. 6. (Color online) The temperature dependence of the susceptibility calculated for the four different domain configurations discussed in the text. The field is applied along [001].

of the field (experimentally of the order of 5 T), the unfavorable structural domain with $\mathbf{Q}_\alpha$ parallel to the field is going to disappear whereby the susceptibility is calculated to show an additional 20% increase (at the lowest temperatures). This is the scenario when increasing the field. When lowering the field, only the two favorable structural domains, with $\mathbf{Q}_\alpha$ perpendicular to the field, are going to be present, but since the system was heated to above T_N each time the field was changed, the magnetic domains with the type I moment perpendicular to the field will also be present at the lowest values of the field. Gardiner *et al.*[7] introduced the notation D_α^β for a domain with the magnetic, type I, ordering vector along the α direction and the spins along the β direction. Using this notation, then the different domain configurations are $\frac{1}{6}(D_a^b+D_a^c+D_b^a+D_b^c+D_c^a+D_c^b) \rightarrow \frac{1}{6}(2D_a^c+2D_b^c+D_a^a+D_c^b) \rightarrow \frac{1}{2}(D_a^c+D_b^c)$ when increasing the field along c from zero to about 5 T (corresponding to the sequence black→green →violet in Fig. 6). For decreasing values of the field, the sequence is $\frac{1}{2}(D_a^c+D_b^c) \rightarrow \frac{1}{4}(D_a^c+D_a^b+D_b^c+D_b^a)$ (violet →yellow). The variations of the calculated susceptibilities at the various values of the applied field are shown in Fig. 6, and they agree in most details with the experimental results presented by Gardiner *et al.*[7] in their Figs. 9(a) and 9(b). This agreement also includes the behavior of the diffraction peaks as function of the applied field—the argument is the one already presented by Gardiner *et al.*

When the field is applied along the [011] direction, the model predicts that this would favor the one domain, where $\mathbf{Q}_\alpha$ is perpendicular to both the y and the z direction, i.e., the $\mathbf{Q}_x$ structural domain. The predictions are qualitatively equivalent to those made when the field is applied along [001]; the only difference of importance is that there should be only one structural domain at high fields and thus only a single susceptibility branch under the decreasing-field condition. The behavior of the neutron-diffraction intensities at 1.55 K observed,[7] when reducing the field to about 0.5 T, after the application of a field of 5 T, is consistent with the transition predicted by the model: $\frac{1}{6}(D_a^b+D_a^c+D_b^a+D_b^c+D_c^a+D_c^b) \rightarrow \frac{1}{2}(D_a^b+D_a^c)$. The diffraction experiments show that the application of a field of the order of 5 T along [011] causes an irreversible change of the structural domain distribution in the antiferromagnetic phase. Nevertheless, the susceptibility changes in a reversible way, not irreversibly as when applying the field along [001], and in the paramagnetic phase (at 20 K), the experimental susceptibility shows no field dependence.[7] This constancy of the susceptibility indicates that the energy benefit of the $\mathbf{Q}_x$ domain must be small and therefore that the [011] field probably leaves the structural domain distribution more or less undisturbed above T_N. The field changes the structural domain distribution in the antiferromagnetic phase, but without any noticeable effect on the susceptibility. The susceptibility is changed alone in a reversible way, which, for most part of it, has to be related to a gradual modification of the magnetic ordering, where the polarization vector of the type I component, with $\mathbf{q}$ along x, is observed to rotate so to become parallel to the field, along [011], at the maximum field. This observation is particularly surprising and is in sharp conflict with the predictions of the model. The energy gain due to the magnetic anisotropy within the plane perpendicular to $\mathbf{Q}_x$ is completely averaged out if the ordering component is polarized along [011].

The rotation of the polarization vector of the magnetic type I moment, when the field is applied along [011], suggests that the in-plane anisotropy is less pronounced than predicted by the model. The rather large rotation of the total ordered moments away from the easy ⟨011⟩ directions in the zero-field case gives the same indication. It has been possible to account for the latter property, but only by introducing an unrealistically large difference between $J((1,0,0))$ and $J(\left(\frac{1}{2},0,1\right))$. Many modifications of the model have been considered, but it is found to be impossible to combine the requirement of an easy plane anisotropy with the requirement that the anisotropy should stay small within this plane. According to the point-charge model, $\eta \simeq -0.002$ in Eq. (17), but although this higher-order term has some effects, it does not give rise to any substantial improvements and, for simplicity, it is left out of the final model. The assumption of a double- or triple-Q structural ordering leads to a more complex anisotropy, and it becomes easier to rotate the moments in the zero-field configuration; however, these structures have other disadvantages. It becomes difficult to reproduce the observed behavior of the domains when the field is applied along [001], and there is no improvement in the account of the observations made when the field is applied along [011]. A multiple-Q deformation of the lattice does not give rise to a multiple-q ordering of the magnetic moments but leads to an additional ordering of the third component of the moments at $\mathbf{q}=\left(\frac{1}{2},\frac{1}{2},0\right)$ (when E_{xz} and E_{yz} are nonzero) with a length μ_3 nearly as large as the length μ_2 of the $\mathbf{q}=\left(\frac{1}{2},0,1\right)$ component. This third component has not been detected in the diffraction measurements, which is an indirect evidence for the single-Q ordered structural phase. The symmetry of this phase, combined with the fact that the type I wave vector is uniquely determined by $\mathbf{Q}_\alpha$, consequently implies a single-q ordering of the antiferromagnetic moments.

The low-energy scattering due to the spin waves in the antiferromagnetic phase was measured by Boothroyd *et al.*[3] The polycrystalline spectrum at 10 K shows a peak centered at about 2.7 meV with a width of the same order of

magnitude.[16] The center of this peak should be close to the mean-field splitting of the paramagnetic ground-state doublet levels, and the model predicts this splitting to be 1.8 meV at 10 K and to saturate at a value of about 2.3 K in the zero-temperature limit. The calculated mean-field splitting is about 30%–40% smaller than the observed one at 10 K. This is surprising since the calculated antiferromagnetic moment, and therefore presumably also the corresponding exchange field, is 40% larger than indicated by observations.

V. CONCLUSION

The present mean-field model accounts in a reasonable way for the properties of PrO_2 in its paramagnetic phase. The analysis predicts that the chiral oxygen displacement model in Fig. 1(b) should be the stable one. The accurate synchrotron x-ray diffraction experiments of Webster *et al.*[8] show that the higher-order scattering peaks and intensities are concordant with this structure, and the presence of the simple sheared structure in Fig. 1(a) can be dismissed. The comparison between the calculated and experimental high-temperature susceptibilities is not entirely satisfactory, but some of the discrepancies may be due to experimental difficulties in obtaining crystals with the right oxygen concentration. The temperature dependent position of the Γ_7 peak agrees in an acceptable way with that derived from inelastic scattering of a polycrystalline sample. The static and the dynamic Jahn-Teller interactions are assumed to have a common origin, the energy scale of which is settled by the transition temperature T_D. The dynamical coupling constant G used in the model calculations is estimated to be of the right order of magnitude in comparison with the static displacements, and multiphonon states have been included in the account of the dynamics. Within the nondispersive approximation, the predicted low-frequency part of the polycrystalline spectrum has qualitative similarities with observations but is far from being an acceptable quantitative estimate. This indicates that the dispersive modifications of the Jahn-Teller interaction need to be considered.

The model correctly predicts a number of the properties of the antiferromagnetic phase but totally fails with respect to reproducing the spin-flip transition detected when applying the field along [011]. The ratio between the two components of the antiferromagnetic moment is close to the observed value, but this is obtained only by invoking an unrealistically large difference between $J((1,0,0))$ and $J(\left(\frac{1}{2},0,1\right))$, and the calculated size of the moment is about 40% larger than observed. The size of the moment is reduced due to the mixing of the phonon and the magnetic states deriving from the dynamical Jahn-Teller interaction. An estimate isolating this particular effect indicates the JT reduction to be of the order of 5%. An increase of the JT coupling parameter does not necessarily lead to a smaller antiferromagnetic moment, as this tendency is nearly compensated for by the need for increasing the exchange interaction, in order to keep T_N fixed.

The field-dependent domain effects observed by Gardiner *et al.*[7] are mostly consistent with the assumption that both the crystallographic JT ordering and the antiferromagnetic one are single-Q structures. The second component of the antiferromagnetic moment is observed at $\langle\frac{1}{2}01\rangle$, not at $\langle\frac{1}{2}00\rangle$, which implies that the magnetic type I wave vector is uniquely determined by the structural one [(1,0,0) if the structural wave vector is $\mathbf{Q}_x$]. The presence of double- or triple-Q crystallographic structures would give rise to a third antiferromagnetic component at the wave vectors $\langle\frac{1}{2}\frac{1}{2}0\rangle$. This component is absent in the diffraction experiments, which indicates that the structural phase is a single-Q one, and the same is then also true for the antiferromagnetic ordering. Hence, this circumstance strengthens the indications that the structures are single-Q ones.

The deficiencies in accounting for a number of the properties of the antiferromagnetic phase indicate that the magnetic two-ion part of the Hamiltonian contains other terms in addition to the superexchange interactions introduced by Eq. (22). The similarities between this system and the actinide dioxides suggest that it may be relevant to supply the even-rank electrical multipolar interactions, responsible for the Jahn-Teller effects, with odd-rank magnetic multipolar interactions, such as those considered in the case of NpO_2.[2] Such couplings would not affect the paramagnetic properties but would change the effective magnetic anisotropy in the antiferromagnetic phase. A change of the anisotropy conditions would influence the total magnitude of the antiferromagnetic moment, the spin wave energies, or the mean-field splitting of the paramagnetic ground-state doublet, and the easy direction may become susceptible to the application of a field.

ACKNOWLEDGMENTS

Carol Webster and Andrew Boothroyd are gratefully acknowledged for stimulating discussions and for their many constructive advices with respect to the interpretation of the neutron scattering data.

[1] S. B. Wilkins, R. Caciuffo, C. Detlefs, J. Rebizant, E. Colineau, F. Wastin, and G. H. Lander, Phys. Rev. B **73**, 060406(R) (2006).
[2] P. Santini, S. Carretta, N. Magnani, G. Amoretti, and R. Caciuffo, Phys. Rev. Lett. **97**, 207203 (2006).
[3] A. T. Boothroyd, C. H. Gardiner, S. J. S. Lister, P. Santini, B. D. Rainford, L. D. Noailles, D. B. Currie, R. S. Eccleston, and R. I. Bewley, Phys. Rev. Lett. **86**, 2082 (2001).
[4] G. A. Gehring and K. A. Gehring, Rep. Prog. Phys. **38**, 1 (1975).
[5] C. H. Gardiner, A. T. Boothroyd, S. J. S. Lister, M. J. McKelvy, S. Hull, and B. H. Larsen, Appl. Phys. A: Mater. Sci. Process. **74**, S1773 (2002).
[6] C. H. Gardiner, A. T. Boothroyd, P. Pattison, M. J. McKelvy, G. J. McIntyre, and S. J. S. Lister, Phys. Rev. B **70**, 024415 (2004).
[7] C. H. Gardiner, A. T. Boothroyd, M. J. McKelvy, G. J. McIntyre, and K. Prokes, Phys. Rev. B **70**, 024416 (2004).
[8] C. H. Webster, L. M. Helme, A. T. Boothroyd, D. F. McMorrow,

S. B. Wilkins, C. Detlefs, B. Detlefs, R. I. Bewley, and M. J. McKelvy, Phys. Rev. B **76**, 134419 (2007).
[9] S. Kern, C.-K. Loong, J. Faber Jr., and G. H. Lander, Solid State Commun. **49**, 295 (1984).
[10] M. T. Hutchings, Solid State Phys. **16**, 227 (1964).
[11] J. Jensen and A. R. Mackintosh, *Rare Earth Magnetism: Structures and Excitations* (Clarendon, Oxford, 1991), http://www.nbi.ku.dk/page40667.htm
[12] J. Jensen, Phys. Rev. B **37**, 9495 (1988).
[13] G. Bevilacqua, D. Ippolito, and L. Martinelli, Phys. Rev. B **69**, 155208 (2004).
[14] S. Kern, J. Chem. Phys. **40**, 208 (1964).
[15] J. B. MacChesney, H. J. Williams, R. C. Sherwood, and J. F. Potter, J. Chem. Phys. **41**, 3177 (1964).
[16] C. H. Webster and A. T. Boothroyd (private communication).